



Visualization and prediction of TVB-N content in chilled pork by hyperspectral imaging

Xiaoyang XING¹ , Maocheng ZHAO^{1*}, Liang QI¹, Yuweiyi TANG¹, Xiwei WANG¹

Abstract

TVB-N is one of the important indexes of the freshness of chilled pork. To present the freshness more accurately and completely, a visualization technology of chemical composition was applied and optimized for pork freshness detection. Two hyperspectral cameras covering visible and near-infrared wavebands were used to detect the TVB-N content. GA, SPA, iPLSR, and siPLSR were employed to select characteristic wavebands from the spectra data extracted from the hyperspectral images, and PLSR models were established on full wavebands and characteristic wavebands. According to the models established on the spectral data, TVB-N distribution maps were obtained, and URV and ICV were employed to evaluate the performance of distribution maps. The results showed that, both PLSR models established on the characteristic wavebands and full wavebands achieved good accuracy, and that the characteristic wavebands cluster was in the spectral range of 600-750 nm, 1020-1120 nm, and 1450-1570 nm. To optimize the performance of distribution maps, prediction models were reconstructed under the guidance of URV and ICV. This study provided a method of predicting TVB-N content of pork in both spectral and imaging aspect for online testing the freshness of chilled pork, which improves the efficiency and quality of testing.

Keywords: chilled pork; TVB-N, visualization; PLSR; hyperspectral imaging.

Practical Application: This manuscript is relevant for the chilled pork production industry, especially for the online testing of the TVB-N distribution of chilled pork. This study provide online testing data on chilled pork and establishes an online test method of freshness of chilled pork. The method provide technical support and a theoretical basis for precision testing of chilled pork.

1 Introduction

Pork constitutes a large part of human diets, and large quantities of pork are consumed globally every year (Duong et al., 2022). Pork contains protein, fat, and vitamins (Alfaia et al., 2019; Duffy, et al., 2018). The protein is very perishable, eating rotten pork will seriously affect human health (Zhang et al., 2019). So the freshness of pork has become the focus of consumers' attention (Liu et al., 2019). In order to maintain the freshness of pork to ensure human safety, many fresh-keeping methods are used on pork, and there are many types of pork on the market (Ribeiro et al., 2019; Zhu et al., 2020). Chilled pork is the most special and common one, which is preserved at 0-4 °C within 24 hours after being slaughtered (Cui et al., 2021). It has been widely purchased by consumers because it maintains the original flavor of the meat without complicated treatment. But because of its simple preservation method, it becomes more perishable. Demand for safe and high-quality meat is growing, not only because of rising living standards but also consumer concerns about food safety (Leng et al., 2020). The detection of pork freshness has always been an area closely related to human life and health (Zhuang et al., 2022).

The testing technology of pork freshness in the laboratory has been developed and improved significantly over a long period of time (Tan et al., 2022). However, most of these methods are time-consuming and have high requirements for

operators (Baek et al., 2021). Some polluting or even harmful substances will be produced during the detection process, e.g. bacteria (Cui et al., 2022), and they are destructive to the pork. However, the traditional pork freshness method carried out in the laboratory is only suitable for sampling detection of pork, not for rapid, nondestructive, and accurate detection. A variety of non-contact detection methods have been developed and used, among them hyperspectral imaging technology is a typical one (Kademi et al., 2019; Xu et al., 2018; Pereira et al., 2021; Ghasemi-Varnamkhashti et al., 2018; Zhang et al., 2022).

Hyperspectral imaging technology is a detection method that can obtain spectral and spatial information at the same time. The hyperspectral image can present the spectral information of objects in the form of images, and each pixel in the hyperspectral image has a corresponding pixel spectrum at its location (Huang et al., 2018). Hyperspectral imaging technology has been used in a variety of fields and can be competent for defect detection and internal content detection (Jiang et al., 2022; Antequera et al., 2021). Internal content detection is based on the response of the object in the corresponding wavebands and establishes the prediction model on the spectral information and the content index to realize the detection, which has been used in the prediction of the freshness of pork (Kucha et al., 2021). Due to the similar function with the spectrometer, the spectral

Received 10 Jan., 2023

Accepted 30 Jan., 2023

¹College of Mechanical and Electronic Engineering, Nanjing Forestry University, Nanjing, China

*Corresponding author: mczhao@njfu.edu.cn

data extracted from the hyperspectral image can establish a corresponding relationship with the total volatile basic nitrogen (TVB-N) content and thus generate a prediction model. Compared with the spectrometer, this method can obtain all the spectral information of the object, which helps the research be more comprehensive and objective.

The spectral information obtained by the hyperspectral camera can describe the complete spectral characteristics of the object, it can only be used to predict the overall TVB-N value of pork when the mean spectrum is used for prediction. When pork spoilage exists only in local areas, the overall freshness prediction value cannot represent the true freshness of pork. In order to predict the distribution of TVB-N content in chilled pork, the TVB-N visualization technology on pork has been developed over the past several years, which brings hyperspectral imaging technology into a new field (Wang et al., 2013). At present, a large number of studies have proved the feasibility of visualization of TVB-N content in pork (Torres & Amigo, 2020). The prediction of TVB-N content at the pixel level with this method is displayed in the form of pictures, which represents the freshness of pork more intuitively.

Hyperspectral imaging system is precise also expensive. If it is used for online nondestructive testing of agricultural and forestry products with low added values, it will face problems such as high price, slow speed, and high computational cost. Thus, it is necessary to establish a multispectral system based on the selected wavebands to meet the demands. However, there are very few studies conducted on the visualization of TVB-N content in chilled pork based on characteristic wavebands.

In the existing research of pork freshness visualization, the original spectral images are usually processed to improve the visualization effect. However, it will have a certain impact on pork freshness prediction, even deviation. At present, no effective analysis of the spatial state of pork freshness visualization has been reported. In fact, a TVB-N content distribution map is also an image that requires simultaneous analysis of the accuracy and distribution of the predicted values. At present, mainly through the visualization effect of people's sensory perception, quantitative analysis methods are still lacking.

The multispectral detection system for TVB-N content in pork has been studied. Most of the multispectral imaging systems are mainly established based on the selected characteristic bands. This method can achieve rapid detection of pork freshness at a relatively low cost. However, there are still few studies on the visualization of pork TVB-N content based on characteristic bands. In order to finally realize the real rapid nondestructive testing, the research on the visualization of pork TVB-N content based on the characteristic wavebands needs to be carried out. The research on full wavebands and characteristic wavebands can provide a strong theoretical basis for the visualization of pork TVB-N content.

In this paper, the accuracy relationship between the freshness prediction models based on hyperspectral and their visualization under the two bands of VIS-NIR and SW-NIR and their combined bands were studied. Through quantitatively evaluating the visualization results and exploring ways to

improve the visualization effect, it can help to lay a foundation for the establishment of a multi-spectral system suitable for the freshness detection of agricultural products.

2 Materials and methods

2.1 Meat materials and sample preparation

Five pieces of fresh pork longissimus muscles were purchased from the local market (Nanjing, Jiangsu Province, China). Each piece of pork was minced into 20 meat slices with a thickness of about 1 cm. All samples were transported to the laboratory in an incubator at about 4 °C, and then each slice was packaged with plastic wrap and stored in a refrigerator at 4 °C. In the subsequent test, 2 slices were taken out daily from each piece of longissimus muscles for TVB-N measurement. The test was conducted for 10 days. Before each experiment, the pork slices were placed in the air for 30 minutes to eliminate the water adhering to the surface.

2.2 Reference measurement

TVB-N content in pork samples is employed as the indicator to represent the pork freshness. The images of each sample were corresponding to the TVB-N content values tested through the semi-micro Kjeldahl method based on the Chinese National Standard GB 5009.228-2016 (Frank et al., 2019). The TVB-N content value can be calculated by the following Equation 1:

$$\text{TVB-N} = \frac{(V_1 - V_2) \times c \times 14 \times 100}{m \times \frac{5}{100}} \quad (1)$$

where TVB-N (mg/100 g) is the content of the meat sample, V1 (mL) is the consumption of HCl by the meat filtrate, V2 (mL) is the consumption of HCl by the blank water, c (mol/L) is the concentration of the HCl, and m(g) is the mass of the meat.

2.3 Hyperspectral image acquisition and optimal spectral data extraction

Hyperspectral image system

A non-destructive testing system was established for acquiring hyperspectral images in this study. There are two hyperspectral cameras, a lighting system, a dark chamber, an uninterruptible power supply (UPS, C3K, SANTAKUPS, China), and a computer in this system. The two hyperspectral cameras are a visible near-infrared camera (VIS-NIR) and a short-wave near-infrared camera (SW-NIR), with a spectral range of 550 to 1000 nm and 900 to 1700 nm, respectively. With those two cameras, hyperspectral images with a range of 550 to 1700 nm could be obtained. The VIS-NIR camera is an assembled camera that comprises an acousto-optic tunable filter (AOTF Camera Video Adapter CVA-200, BRIMEROSE, USA), a visible near-infrared camera (ORCA-R², HAMAMATSU, Japan), and a zoom lens (Nikon, AFS NIKKOR 18-200 mm 1:3.5-5.6G ED VR II, Japan). The SW-NIR camera is a kind of linear array hyperspectral camera (GaiaField-V10E-AZ4, Jiangsu Dualix Spectral Image Technology Co. Ltd, China), which has an internal push sweep device inside. Hence, these

two cameras with different acquisition modes can capture the image of the sample on the same platform. The lighting system includes 12 halogen lamps (50W, Philips GU5.3, China), which were supplied by a UPS, and the system was surrounded by a dark chamber. In order to isolate the influence of external light, the system is surrounded by a dark chamber.

Acquisition of hyperspectral images and hyperspectral curves

The VIS-NIR hyperspectral camera captured images with 672×512 pixels by applying variable exposure mode. The spectrum interval of each channel was 3 nm, and there were 141 channels in each image. The SW-NIR hyperspectral camera captured images with constant exposure mode, and the resolution of the images was 550×640 pixels. The spectrum interval of each channel was 1.7 nm, and there were 512 channels in each image.

To minimize the effects of environmental factors on hyperspectral images, dark and white reference images were captured before tests. Hence, there were two reference images corresponding with every hyperspectral image. A hyperspectral reflectivity image can be computed by the following Equation 2

$$R = (R_r - R_d) / (R_w - R_d) * C \quad (2)$$

Where R is the hyperspectral reflectivity images of the sample; R_r is the raw hyperspectral image of the sample; R_w is the white reference hyperspectral images of the standard reflectivity board (SRT-99-100, Labsphere, USA); R_d is the dark reference image acquired by completely blocking the lens with an opaque cap; C is the standard data of the standard reflectivity board.

The region of interest (ROI) is commonly used for the establishment of prediction models. Nowadays, ROIs were the whole regions of the samples, rather than a local region on the surface of samples, which differs the hyperspectral imaging technology from the near-infrared spectrometer technology. There are numerous methods to acquire ROIs. In this study, a traditional method was implemented to separate the sample region from the background region. A threshold segmentation algorithm was used to acquire the basic ROIs. By modifying on the basic ROIs with the methods of image expansion and corrosion, the mask of the meat region can be obtained.

Selection of characteristic wavebands

Compared to the model established on the full waveband data acquired from the hyperspectral camera, a lower spectral dimension is a better choice (Shen et al., 2020). Genetic algorithm (GA) is a characteristic wavebands search method that simulates natural selection and genetic process in the Darwinian model (Wei et al., 2022). In this study, the spectral data were treated as chromosomes and the wavelengths were treated as genes. By minimizing the cost function with the genetic operations of selection, crossover, and mutation, the characteristic wavebands could be selected. Successive projection algorithm (SPA) is a forward selection algorithm, which projects the spectral data to a lower space to select the wavebands with the characteristics of small collinearity and low redundancy (Tang et al., 2021; Yang & Kan, 2020). Interval partial least square regression (iPLSR) is a method that based on PLSR, which divides the spectral

data into equal width interval in the dimension of spectrum (Kiala et al., 2017). In this study, the spectral data with a step of specific length of wavebands were divided into the intervals for modeling. The characteristic wavebands could be selected by the values of RMSE. Meanwhile, synergy interval partial least square regression (siPLSR) was adopted to select characteristic wavebands, which can select two intervals from the spectral data.

2.4 Establishment of prediction models

In this study, partial least square regression (PLSR) was used to establish the prediction model for TVB-N content in chilled pork. PLSR is a model that combines principal component analysis, canonical correlation analysis, and multiple linear regression, which projects prediction variables and observation variables into a new space to find the relationship between the two. PLSR is a traditional method, which has been used widely and has a high performance. During the process of establishing prediction models, 5-fold cross-validation was adopted. The performance of each model was calculated by root mean square error (RMSE) and coefficient of determination (R^2). A model with a higher R^2 , and a lower RMSE was considered as an optimal model.

2.5 Visualization method of TVB-N distribution and optimization

By computing the mean pixel value, the spectral data were obtained representing the sample, and the pixel in this same position of the image also represents the spectral information of this position. So, pixel spectral data were the same as the spectral data extracted from the image, which can be brought into the Formula 3 that represents the spectral model to obtain the prediction value of the pixel. The visualization of TVB-N will be generated by this way, which is defined as follows:

$$TVB-N_{pixel} = f_{spec}(\text{spec}_{pixel}) \quad (3)$$

Where spec_{pixel} represents the spectral data of pixels in the ROI of hyperspectral images, f_{spec} represents the formula of the TVB-N prediction models established on the spectral data and TVB-N values, $TVB-N_{pixel}$ represents the TVB-N prediction values of the pixel in the ROI.

To make a further study in visualization of TVB-N distribution, unreasonable values ratio (URV) and inverse coefficient of variation (ICV) were used to represent the performance of visualization models.

For the reason that the TVB-N values represent the total volatile basic nitrogen content in the chilled pork, the TVB-N values should be larger than 0 mg/100 g. When the TVB-N prediction value is lower than 0 mg/100 g, it means that the prediction value is in the unreasonable range. Besides, the chilled porks were stored for 10 days, the TVB-N content would not be too large, and the reasonable prediction values were set under 300 mg/100 g. As a result, the TVB-N prediction values, which is in the range of 0-300 mg/100 g, were judged as reasonable prediction values. The Formula 4 of URV is defined as follows:

$$URV = \frac{n_{ur}}{n_{roi}} \times 100\% \quad (4)$$

Where n_{ur} and n_{roi} represent the Number of unreasonable pixels and the number of all pixels in ROIs, respectively. The closer the value of URV is to 0, the better the visualization result is; and the closer it is to 1, the worse the visualization result is.

ICV is usually used to describe the noise level of images taken in the field of hyperspectral and multispectral remote sensing imaging. In visualization, if the difference between adjacent pixels is large, the noise in the region will be large, thus losing the contour features that the original spectral image should have. This study introduced this index to evaluate the visualization effect to evaluate the volatility of the predicted values in the visualization results. The ICV can be defined as Formula 5 (Chen et al., 2018):

$$ICV = \frac{R_m}{R_s} \tag{5}$$

Where R_m and R_s are the mean and standard deviation of pixel values, respectively. The larger the value of ICV, the more consistent the predicted values in ROI, and the closer to 0, the greater the difference in the predicted values of ROI.

In this study, URV and ICV were used to evaluate the visualization effect. All data analysis procedures were performed using MATLAB software (Mathworks, Natick, Ma, USA).

3 Results and discussion

3.1 Measurements of TVB-N

10 samples were removed in this study, due to the abnormal chemical values of samples and the damage to some spectral data. A total of 90 samples were used for data analysis. The leave-one-out method divided the data set into a training set and a test set at a ratio of 3:1, as shown in Table 1. It showed that the TVB-N range of the training set completely encompassed the TVB-N range of the testing set, and the two sets had similar

mean values and standard deviation values with the complete data set. Therefore, the method of dataset splitting in this way is reasonable and can be used to verify the reliability of the training set model.

3.2 Spectral characteristics and datasets

The spectra extracted from the image of the VIS-NIR camera and SW-NIR camera are shown in Figure 1. The wavebands of SW-NIR spectra ranging from 874-1023 nm and 1612-1731 nm were removed, because of the low pixel signal noise ratio. Hence, the SW-NIR ranged from 1245-1610 nm. The image quality of the VIS-NIR waveband was good, and the spectral range was still 550-970 nm. In the selected band range, the spectral data of pork had good consistency, which proved that the good quality of spectral data can be used for spectral analysis.

3.3 TVB-N prediction model

Prediction models on full wavebands

PLSR models were established on VIS-NIR, SW-NIR, VIS-NIR and SW-NIR fusion bands, respectively. The results are shown in Table 2. It could be found that the 3 models exhibited similar performance on both the training set and testing set. Compared to the model based on SW-NIR spectral data, the model based

Table 1. Reference measurement of TVB-N content of 90 samples in data sets.

Data set	Number of samples	Range of TVB-N content (mg/100 g)	Mean (mg/100 g)	Standard deviation (mg/100 g)
Total set	90	3.66-26.37	10.96	4.65
Training set	68	3.66-26.37	10.94	4.74
Test set	22	5.24-22.70	11.00	4.45

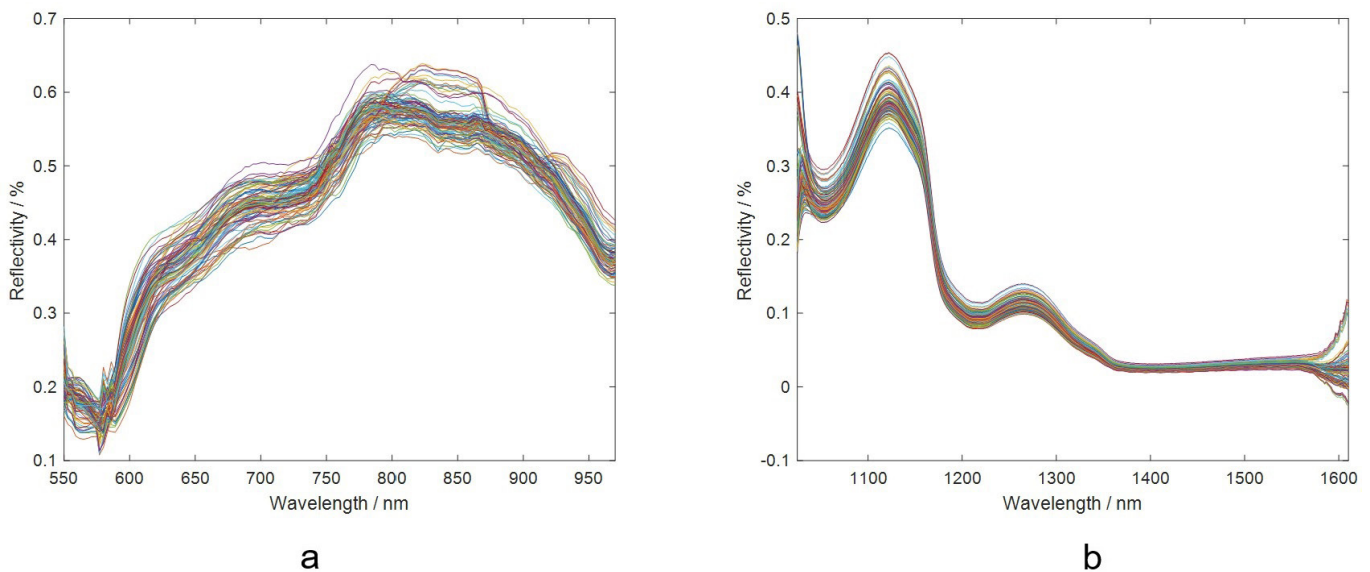


Figure 1. VIS-NIR and SW-NIR spectra of chilled pork. (a) VIS-NIR spectra of samples; (b) SW-NIR spectra of samples.

Table 2. PLSR model results for each indicator.

Wavebands	Number of wavelength	Range of wavebands (nm)	RMSE _c (mg/100 g)	R _c ²	RMSE _p (mg/100 g)	R _p ²
VIS-NIR	141	550-970	1.2340	0.8748	1.8057	0.8274
SW-NIR	350	1024-1610	1.6366	0.8791	1.856	0.8176
VIS-NIR& SW-NIR	491	550-970 1024-1610	1.7891	0.8556	1.7891	0.8305

on VIS-NIR had better performance, which got RMSE_p and R_p² of 1.8057 mg/100 g and 0.8274, respectively. The model based on the spectral data of VIS-NIR and SW-NIR fusion wavebands demonstrated the best performance, whose RMSE_p and R_p² were 1.7891 mg/100 g and 0.8305, respectively. The more spectral information helped the model achieve better performance.

Prediction models on characteristic wavebands

In this study, SPA, GA, iPLSR and siPLSR were used to select characteristic wavebands in VIS-NIR and SW-NIR wavebands, respectively, and TVB-N prediction models were established based on PLSR. The characteristic bands selected by GA and SPA were discretely distributed on the whole band, while iPLSR and siPLSR were continuously distributed on the whole band. In order to analyze the influence of wavelength number in the selected wavebands on the model, the wavelength number in wavebands were set from 10 to 70, and the interval was 10.

The results of GA-PLSR and SPA-PLSR are shown in the Figure 2, where the abscissa in each image represented the number of characteristic wavelengths contained in the characteristic wavebands, and the ordinate indicated the performance of the model. In the VIS-NIR wavebands, when the number of wavelengths was small, the model had a weaker capability for spectral data and TVB-N values. At this time, the performance of the training set was weak than that of the test set, and the performance of the model was unreliable. As the number of wavelengths increased, the performance of the model was gradually improved. The model with the best performance in this band was the one with 30 wavelengths with RMSE_c and R_c² being 1.9537 mg/100 g and 0.8277, respectively, RMSE_p and R_p² being 1.9914 mg/100 g and 0.7900, respectively.

In the SW-NIR spectral data, as the number of wavelengths increased, RMSE_c decreased and R_c² increased, and the relationship between the spectral data and TVB-N improved. RMSE_p and R_p² also showed the same phenomenon, indicating that the prediction model was robust in the test data. When the number of wavelengths reached 50, the performance of the model no longer changed drastically. It can be speculated that when the wavelengths in the selected bands reached a certain number, the model could better predict TVB-N, and when the number continued to rise, it would not have more impact, the performance of the model did not change dramatically, and remained relatively stable. As a result, the best model was established on the band containing 50 characteristic wavelengths with the RMSE_c and R_c² being 1.2765 mg/100 g and 0.9264, respectively, and RMSE_p and R_p² being 1.8188 mg/100 g and 0.8248, respectively. Compared with the model established by SPA on the data of two bands, it

can be found that the effect of model establishment was better on the SW-NIR band.

Different from SPA, GA selected characteristic wavebands based on both spectral data and TVB-N values. These two groups of models showed an increase in performance with the number of wavebands increasing and then decreasing. The model based on VIS-NIR spectral data, achieved the best performance of 1.8770 mg/100 g and 0.9410 for RMSE_c and R_c², respectively, and 1.7726 mg/100 g and 0.9184 for RMSE_p and R_p², respectively, and the number of wavelengths was 30. The model based on SW-NIR spectral data, achieved the best performance of 1.2919 mg/100 g and 0.9376 for RMSE_c and R_c², respectively, and 1.0073 mg/100 g and 0.9296 for RMSE_p and R_p², respectively, and the number of wavelengths was 30.

iPLSR and siPLSR were different from SPA-PLSR and GA-PLSR in the form of selected wavebands. The characteristic wavebands were continuous regions selected from the original wavebands. The results of iPLSR and siPLSR are shown in Figure 3. As the number of wavelengths increased, the performance of the model continued to improve, and then began to decline. The optimal model on the VIS-NIR data was established on the characteristic bands containing 50 wavelengths. The RMSE_c and R_c² were 1.8861 mg/100 g and 0.8395, respectively, and RMSE_p and R_p² were 1.7707 mg/100 g and 0.8340, respectively. The optimal model on the SW-NIR data was established on the characteristic bands containing 60 wavelengths with the RMSE_c and R_c² being 1.7078 mg/100 g and 0.8684, respectively, and RMSE_p and R_p² being 1.7868 mg/100 g and 0.8309, respectively.

Different from iPLSR, siPLSR get two continuous characteristic bands, so the number of wavelength selected by siPLSR was twice that of the other three methods. Due to that, the minimum wavelength number of characteristic bands selected by siPLSR is 20. In the VIS-NIR band, when the number of wavelengths was 40, the model performed similarly on the test set and the training set and was also the best model. The RMSE_c and R_c² are 1.6190 mg/100 g and 0.9827, respectively, and RMSE_p and R_p² are 1.5963 mg/100 g and 0.8651, respectively. In the SW-NIR band, the optimal model was established on the characteristic band containing 30 wavelengths, with the RMSE_c and R_c² being 1.0979 mg/100 g and 0.9456, respectively, and RMSE_p and R_p² being 1.4965 mg/100 g and 0.8814, respectively.

Selection of spectral bands for freshness prediction

Compared with the prediction model established by full-band data, four characteristic wavebands prediction models worked better, and GA-PLSR and siPLSR showed the best performance. It was feasible to use the characteristic wavelengths selected by

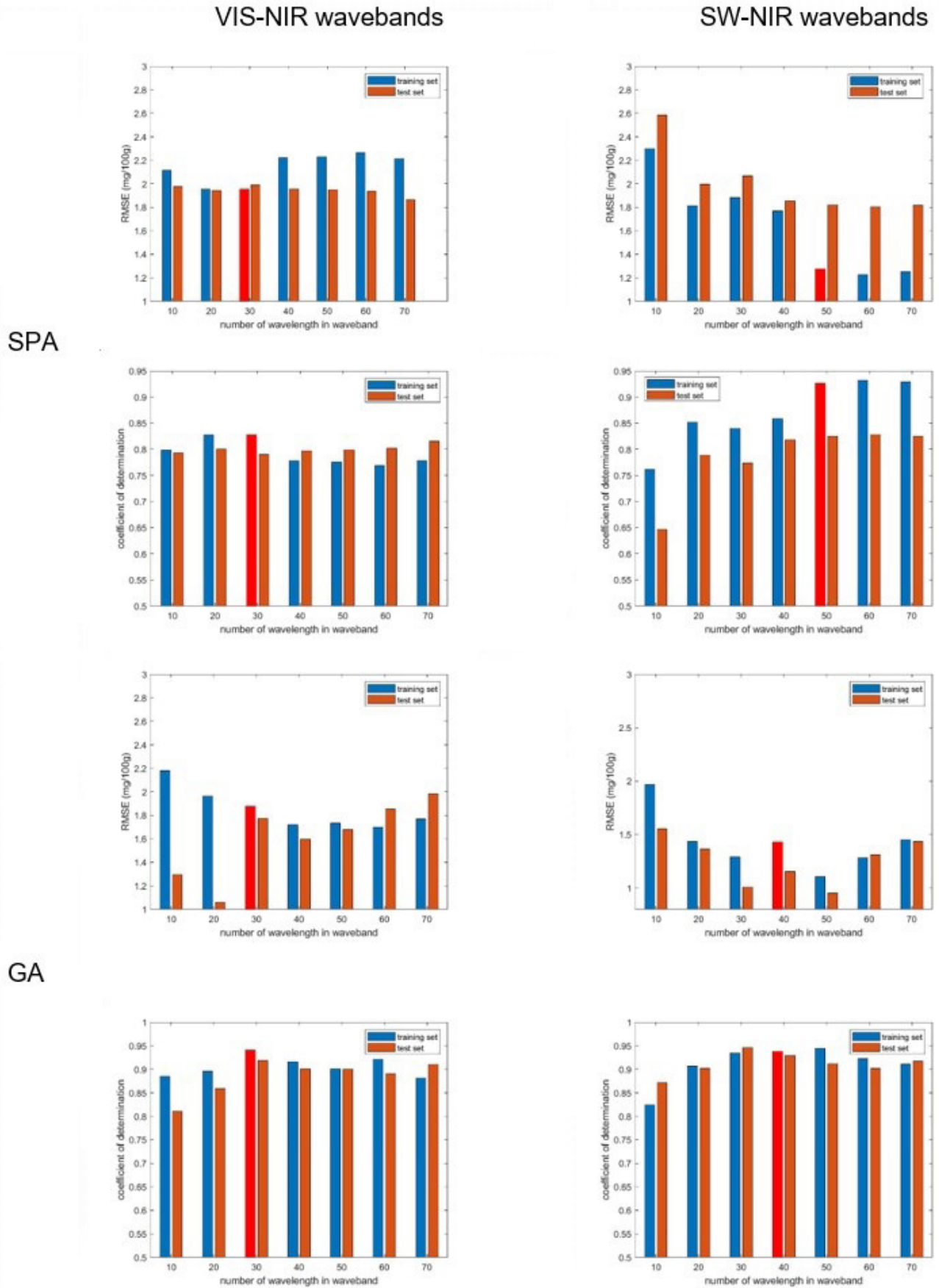


Figure 2. Results of SPA-PLSR and GA-PLSR models on characteristic wavebands with different number of wavelengths.

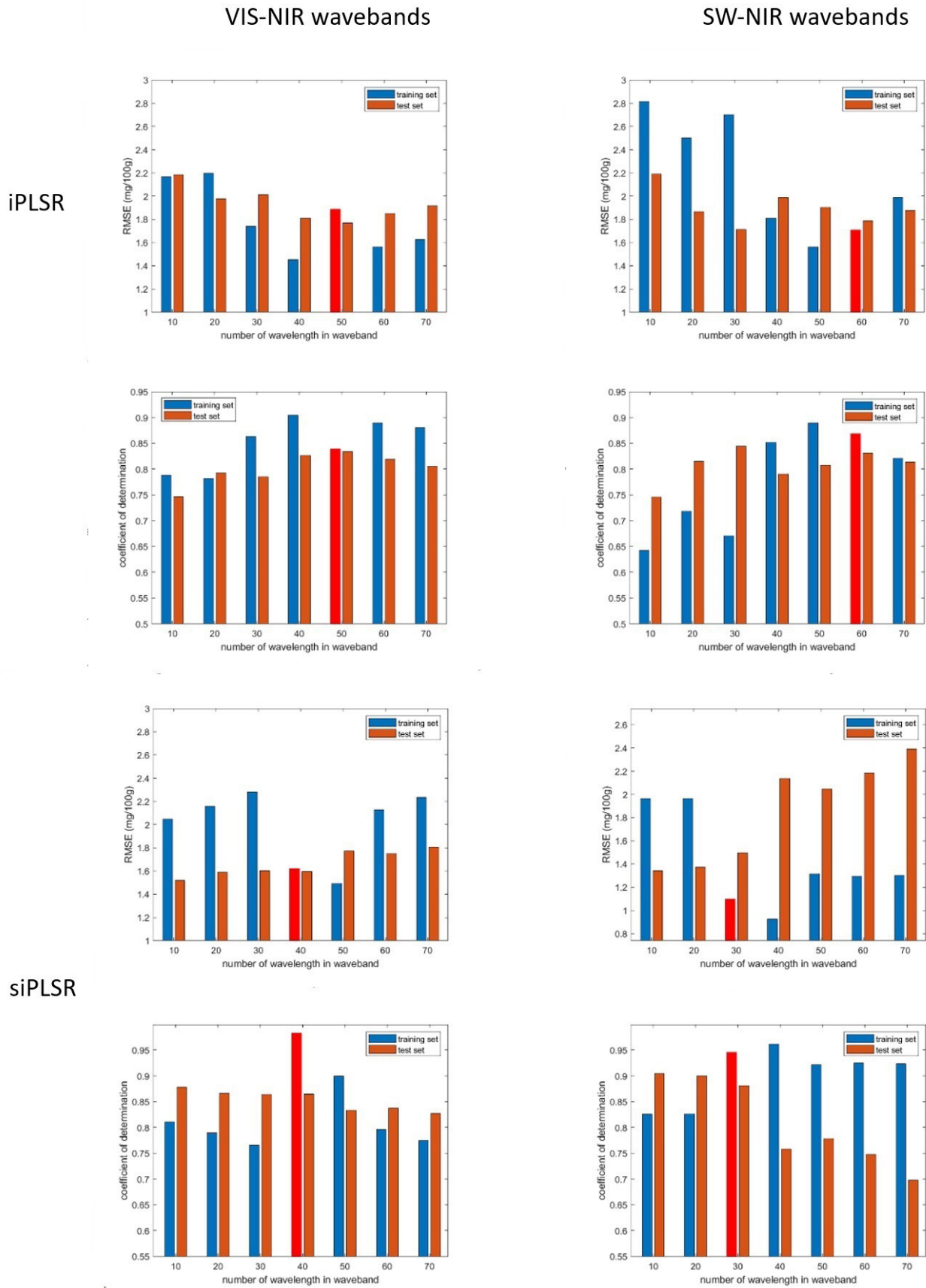


Figure 3. Results of iPLSR and siPLSR models on characteristic wavebands with different number of wavelengths.

those four characteristic band selection methods to establish TVB-N prediction model, which used less data than the model established by full band data, and was more suitable for establishing a rapid TVB-N content detection system for chilled meat. When the number of characteristic wavelengths was small, the model was not able to predict the TVB-N content well. When the number of wavelengths increased, the performance of the model gradually increased. Among them, GA-PLSR was superior to other methods in prediction performance. GA-PLSR could better derive the correlation between TVB-N and spectral data, but the search time for characteristic bands was longer. Compared with GA-PLSR, SPA-PLSR had little improvement in performance, but it took the least time in feature band selection. iPLSR and siPLSR also showed good performance, especially with siPLSR. Through those two methods, it was found that the characteristic bands were concentrated in a specific interval, which was very different from the bands selected by SPA and GA.

The characteristic bands selected by iPLSR and siPLSR were distributed in continuous intervals, which could be used to analyze the relationship between spectral information in continuous bands and TVB-N content in chilled pork. The characteristic bands selected by SPA and GA were discretely distributed in the whole band range, which were not able to form a complete and continuous band for establishing a prediction model. Therefore, this study mainly analyzed the characteristic bands selected by iPLSR and siPLSR, and the results are shown in Figure 4, where the abscissa represents the band range, and the left and right represent the visible near-infrared VIS-NIR and short-wave near-infrared SW-NIR bands, respectively. When selecting the characteristic bands, iPLSR selected two sets of characteristic bands for the characteristic bands containing different characteristic wavelengths for comparison with siPLSR.

In the VIS-NIR band, the band range selected by iPLSR was mainly concentrated on the first half, and when the wavelength

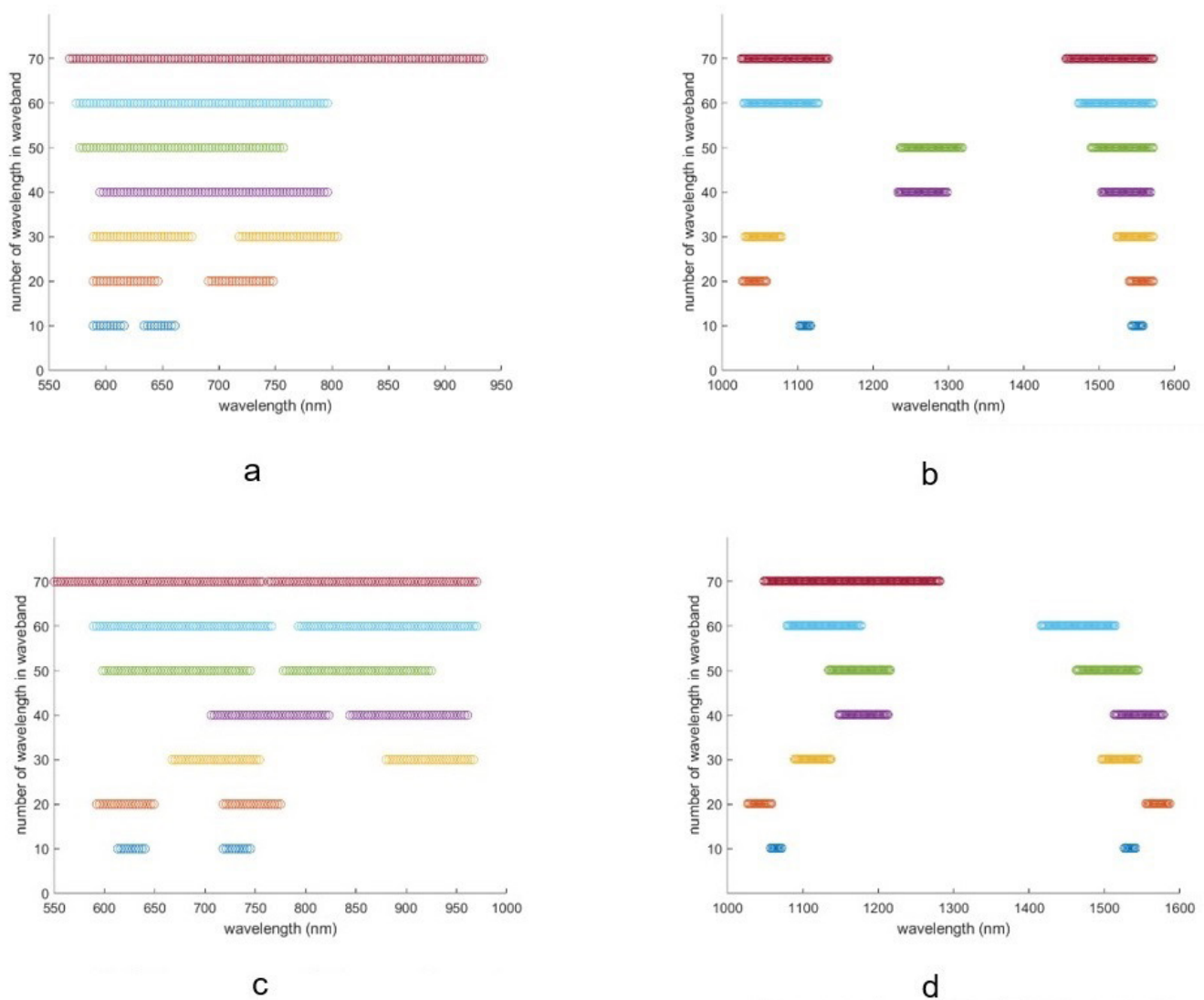


Figure 4. The wavebands selected by iPLSR and siPLSR on VIS-NIR and SW-NIR wavebands. (a) iPLSR on VIS-NIR wavebands; (b) iPLSR on SW-NIR wavebands; (c) siPLSR on VIS-NIR wavebands; (d) siPLSR on SW-NIR wavebands.

was 70, the selected characteristic band was approximately the full band because the number of wave fields in the full band was 141. When the wavelength number was 10, the selected characteristic band was within 600-650 nm. As the number of characteristic wavelengths continued to increase, the characteristic bands were still similar to the bands with a wavelength of 10, mainly covered the range of 600 nm-750 nm. When siPLSR was used to select feature bands, two completely disjoint bands were selected each time, so they were more dispersed. Even that, there are still plenty of selected wavelengths in the 600-750 nm range, except the model established on the bands with 40 wavelengths. Therefore, it can be concluded that the spectral data in the 600-750 nm band range were closely related to the TVB-N content of chilled meat.

In the SW-NIR band, the characteristic bands selected by iPLSR were mainly concentrated on the range of 1020-1120 nm and 1450-1570 nm. Only when the number of wavelengths was 40 and 50, each group of data was not in this range. The characteristic bands selected by siPLSR were also similar to those selected by iPLSR, which were mainly concentrated on the head and tail intervals of the full band, and the spectral ranges were very close. Through iPLSR and siPLSR on VIS-NIR and SW-NIR spectral data, it was found that the TVB-N content of chilled pork had a good correlation with the information in a specific spectral range, which is 600-750 nm, 1020-1120 nm and 1450-1570 nm, respectively. To meet the test speed, a multispectral camera system usually contained several bands. This finding could provide a strong theoretical basis for the establishment of multispectral pork TVB-N online detection system.

3.4 Evaluation of TVB-N distributing map

The models with the strongest performance in PLSR, SPA-PLSR, GA-PLSR, iPLSR and siPLSR prediction models were used for the visualization of TVB-N content spatial distribution. As shown in Figure 5, the upper and lower lines in the figure showed the prediction of TVB-N content distribution of a slice of pork on the first day of VIS-NIR and SW-NIR bands,

respectively. The TVB-N content was represented in pseudo-color, 0 mg/100 g in blue and 20 mg/100 g in red. And the background was set to 0 in the distribution maps. Since the Chinese national standard uses 15 mg/100 g to measure whether pork is edible, 20 mg/100 g was set to a maximum value that highlights the difference between pixels.

As seen from Figure 5, in the SW-NIR band, there were a large number of pure blue and pure red areas in the TVB-N distribution map, indicating that the predicted value of TVB-N was outside the range of 0-20 mg/100 mg, and the contour of pork completely disappeared with a large error, which is different from the TVB-N distribution maps generated on the hyperspectral images of VIS-NIR wavebands. As shown in Figure 6, the PLSR, SPA-PLSR and iPLSR visualization models with better sensory effects in the VIS-NIR band were further analyzed. It can be found from the distribution maps that the TVB-N predicted value of chilled pork increased with the increase of storage days, which was consistent with the reality of pork decay. Pork began to rot from the edge until it finally rotted to the middle. The prediction results of the three models were basically consistent.

All visualization results in the VIS-NIR band were evaluated by URV and ICV. The evaluation results are shown in Table 3. The first five lines indicated the evaluation results of those five models. PLSR was a linear regression model, which means that

Table 3. Evaluation indexes of visualization models.

Methods of modeling	Number of main component	URV	ICV	RMSE (mg/100 g)	R ²
PLSR	4	6.49%	1.9420	1.8057	0.8274
SPA-PLSR	4	6.71%	1.5897	1.8655	0.8157
GA-PLSR	9	31.64%	0.5576	1.1530	0.9296
iPLSR	5	9.43%	1.3941	1.9776	0.7929
siPLSR	9	28.52%	0.6124	1.7729	0.8335
siPLSR	7	9.44%	1.3675	1.8568	0.8174

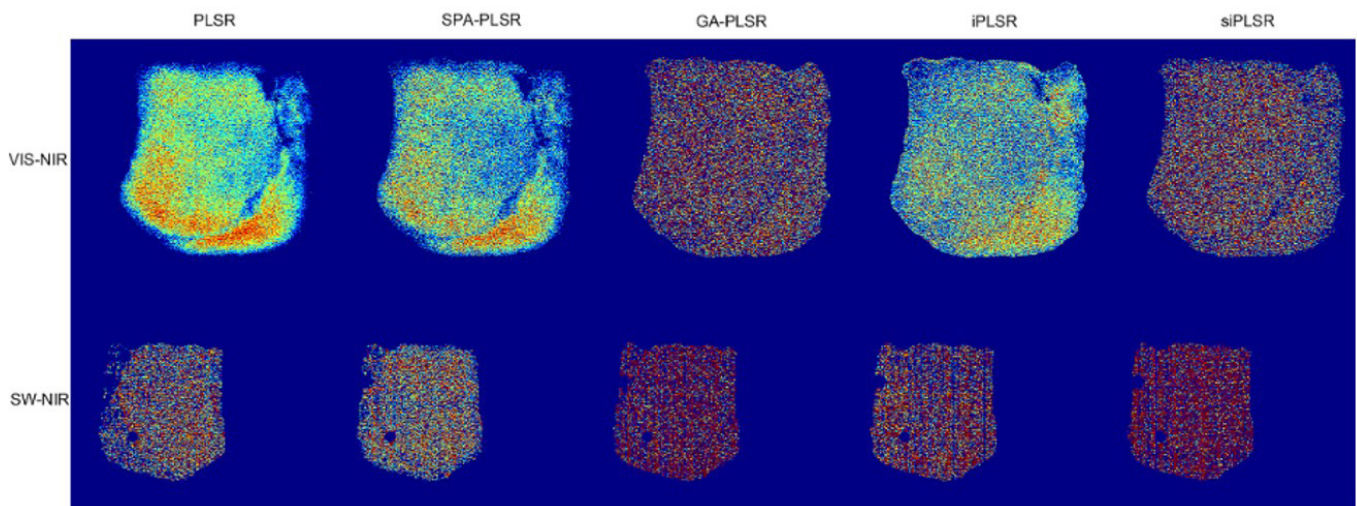


Figure 5. Distributing maps of TVB-N predict values of the five models on VIS-NIR and SWNIR wavebands.

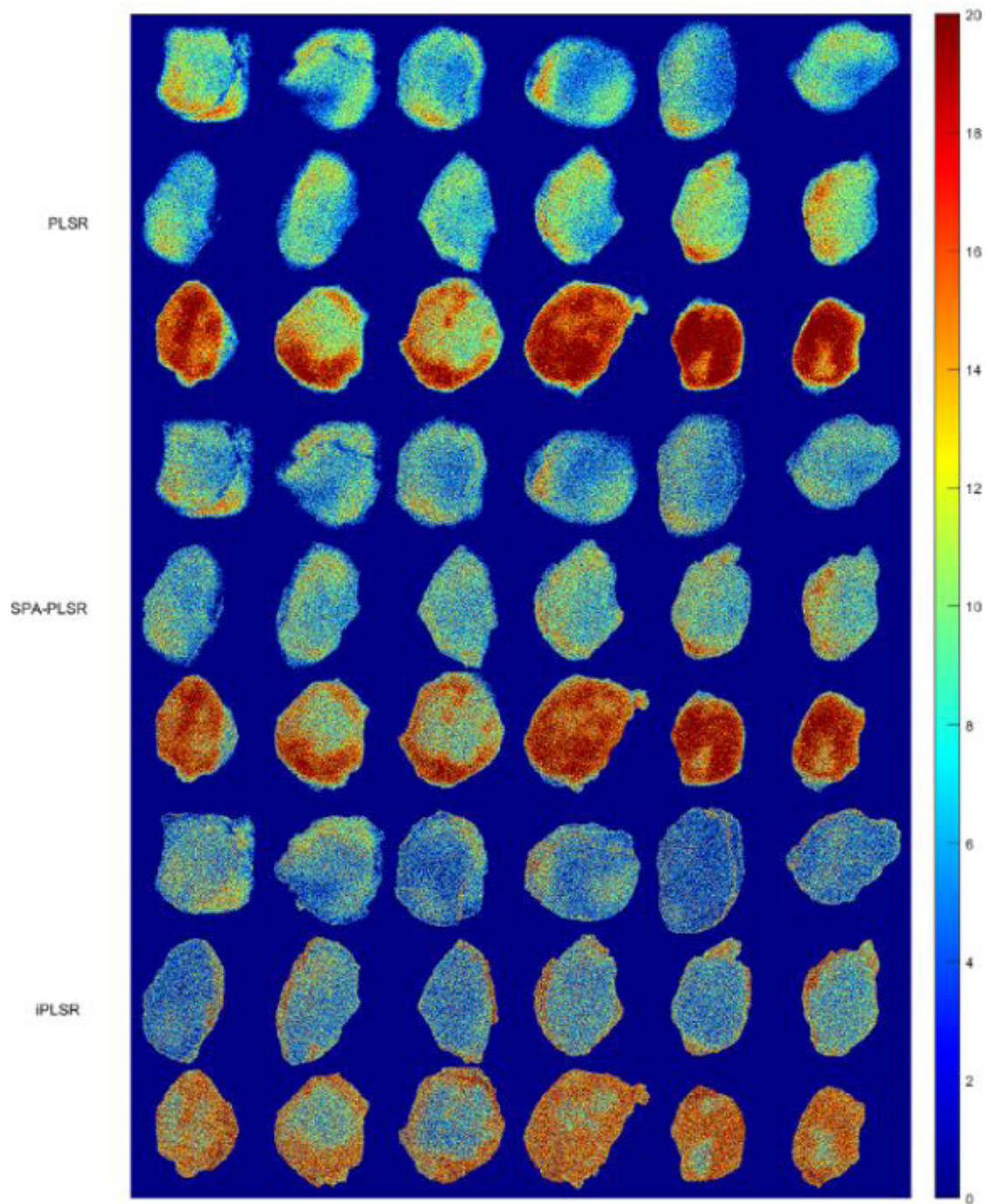


Figure 6. Distribution of TVB-N values of PLSR, SPA-PLSR, and iPLSR during the storage.

the predicted value of the spectral model is the same as the average predicted value of the pixels in the TVB-N distribution. Therefore, although those two indexes were not related to the distribution of TVB-N, they helped measure the accuracy of TVB-N performance. Compared with the other three models, GA-PLSR and siPLSR had a higher UVR greater than 40%. This means that the predicted value of the pixel was not in the range of 0-300 mg/100 g. And the ICV values of those two models were still lower than other models, even less than 1, indicating that the predicted values of TVB-N were scattered. It could be found that

the visualization results established by VIS-NIR full-band data were the best, with a URV value of 6.49% and an ICV value of 1.9420.

The huge difference in Table 3 means that models for visualization could not be selected based on the results of spectral data alone. Spectral data were derived from the average of pixels values in the ROIs, not exactly the same as the pixel spectral data. During the establishment of models, especially GA-PLSR could fit spectral data with TVB-N values to obtain better spectral prediction performance, but failed to guarantee visualization

performance. It could be found that the principal component factors of GA-PLSR and siPLSR were both 9, which was much larger than the principal component factors of PLSR, SPA-PLSR and iPLSR. When the number of principal components was larger, the PLSR model fitted better on the training set. At the same time, there would be over-fitting, namely, the model could not fully fit the spectral information and the TVB-N content of chilled meat on the training set, but it performed poorly on the test set. The number of principal components selected here corresponded to the model that performs best on the test set and the performance of the training set was not weak with the test set, which ensured that the selected model had better performance on the test set and the training set. However, this method could not guarantee the good performance of the model on the TVB-N content distribution maps, and the inconsistency between the pixel spectrum and the mean spectrum made the model unable to accurately predict TVB-N values. Similar to the over-fitting of spectral models, when the performance of the spectral model was excellent but the visualization results were poor, the prediction model was over-fitted on the spectral data. Therefore, the number of principal components of the siPLSR model was reduced to generate a new TVB-N content distribution map. The results are shown in Figure 7a and the sixth row of the Table 3. When the number of principal

components was reduced, the RMSE of the model increased upward, and R^2 decreased, but the overall performance did not decrease much, and did not have much impact on the overall prediction accuracy. In the visual evaluation results, it can be found that the original 28% URV value was reduced to 9.44%, and the ICV value was also increased to 1.3675. By comparing the siPLSR results of Figure 7a and Figure 5, it can be found that the overall color on the optimized visualization map was bluer and the distribution trend was similar to the full-band PLSR results. Therefore, it was feasible to use this method of reducing principal components to enhance the effect of visualization.

The same method was used to optimize the visualization results of SW-NIR band data. The results are shown in Figure 7b and the statistical results are shown in the Table 4. In Table 4, the principal components of PLSR were selected as 6, 7, 8, 9, 10, 11, and 12, respectively, and the best principal component selected by spectral model performance was 11. When the principal component score increased to 12, it means that the model tended to be more over-fitting. At this time, RMSE increased and R^2 decreased, that is, the prediction performance of the model decreased, and the URV value increased and the ICV value decreased. The unreasonable prediction pixels in the TVB-N content distribution maps increased and the correlation

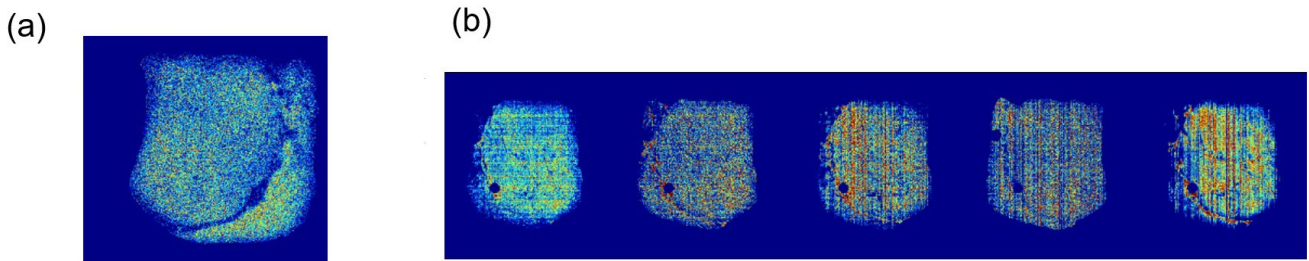


Figure 7. The modified distribution maps of TVB-N. (a) The modified distribution map of siPLSR on VIS-NIR; (b) The modified distribution maps on SW-NIR.

Table 4. The evaluation of the performance of TVB-N distribution maps on SW-NIR.

Methods of modeling	Number of main component	URV	ICV	RMSE mg/100 g	R2
PLSR	12	16.63%	1.0603	2.1176	0.7626
	11	12.33%	1.3189	1.8572	0.8173
	10	8.46%	1.4278	2.1666	0.7514
	9	5.49%	1.5933	2.1020	0.7530
	8	4.93%	1.6002	2.1427	0.7569
	7	4.04%	1.5843	2.4490	0.6824
	6	3.44%	1.5652	2.4950	0.6704
SPA-PLSR	8	8.91%	1.326419	2.1994	0.7438
	9	30%	0.9204	1.8083	0.8268
GA-PLSR	8	15.31%	1.172808	2.0103	0.786
	15	58.43%	0.3039	1.3624	0.9017
iPLSR	7	18.88%	1.044917	2.0658	0.7741
	10	51.24%	0.4406	1.7868	0.8309
siPLSR	4	13.68%	1.08658	2.4172	0.6906
	16	44.85%	0.1321	1.4965	0.8814

between adjacent points on the image decreased. Therefore, when the spectral model tended to be over-fitting, the quality of the visual map tended to be worse. When the number of principal components decreased from 11 to 6, the value of URV began to decrease gradually, which means that there were more predicted values in the TVB-N visualization graph within a reasonable range, and the ICV value also began to increase gradually, which means that the surface of the generated TVB-N visualization graph was smoother and the image quality was improved. This is because when the principal component decreased, the degree of over-fitting of the model began to decrease, but the model tended to be in an under-fitting state, namely, the prediction of pixels tended to be a stable value. By examining the RMSE value and R^2 value in the Table 4, it can be found that the prediction performance of the spectral models began to decrease gradually. When the number of principal components was 6, the RMSE was 2.4950 mg/100 g, and the R^2 was 0.6704, which was significantly lower than the prediction performance of the model with the principal component number of 11. However, when the number of principal components was 8, the prediction performance of the model did not decrease significantly, and the visualization performance was also greatly improved. By analyzing the models with different number of principal components and their visualization effects, this study set the number of principal components used in PLSR model to 8 in order to get a better TVB-N distribution map.

Comparing the effect of the visualization map generated by the SW-NIR band data, it can be found that the visualization results generated by this method were greatly improved compared with the previous ones. Compared with Figure 5, the overall distribution of TVB-N predicted values showed in Figure 7b looked more reasonable. From the data point of view, the URV values of the unadjusted distribution maps were about 40% -50%, which means that half of the predicted value in the image was far from the actual value, and the URV values of the adjusted distribution maps were below 15%, which is a huge improvement compared to the unadjusted before. The ICV value of the unadjusted distribution maps also had tremendous changes compared to before. The original ICV remained basically below 1, or even less than 0.5, which was reflected in the image noise being too large, that is, the predicted value on the image fluctuation range was large and not concentrated. After adjustment, the ICV values were basically greater than 1, so the visualization results of the sensory effect were greatly improved. From the perspective of the number of principal component factors, the number of principal component factors selected by the adjusted model was decreased, and the use of this method would also lead to changes in the RMSE and R^2 values of the model. The RMSE before adjustment was less than 2, while the RMSE after adjustment was greater than 2 mg/100 g. R^2 was originally above 0.8, but after adjustment it was less than 0.8. Therefore, reducing the number of principal components could avoid the over-fitting of the visualization model on the spectral data, and also reduced the performance of the spectral model. An equilibrium point needed to be selected between the two when making visualization predictions. With the above adjustments, a visual prediction of usable TVB-N content could be established on both VIS-NIR and SW-NIR data.

In terms of prediction models established on the mean spectral data, VIS-NIR and SW-NIR have similar performance. However, in terms of visualization results, VIS-NIR waveband data performed better. Therefore, the performance of the spectral model was not consistent with the visualization effect. After adjustment, although the visualization effect of SW-NIR was improved, there was still a significant gap compared with VIS-NIR. Numerically, the URV value of VIS-NIR was basically below 10%, and the ICV value was also greater than 1.3. Most importantly, only siPLSR and GA-PLSR based on VIS-NIR wavebands needed to be adjusted, and the adjusted R^2 was still greater than 0.8, and RMSE was less than 2 mg/100 g. This indicated that the accuracy of the model established using VIS-NIR data was higher than that of SW-NIR.

In summary, a higher performance of the spectral model did not mean a better performance of the visualization model. In order to generate a TVB-N distribution map with high imaging quality and high prediction performance, it was necessary to select a model that can fit the TVB-N values in both the spectral model and the visualization model.

4 Conclusions

In this study, hyperspectral imaging technology and chemometrics methods were used to predict the freshness of chilled pork. URV and ICV were employed to evaluate the effect of TVB-N distribution maps, and a method was designed to modify the visualization results. The following conclusions can be drawn: 1) VIS-NIR camera with a spectral range of 550-970 nm and SW-NIR camera with a spectral range of 900-1700 nm had the ability to predict TVB-N content in chilled pork; 2) The prediction models established by the characteristic wavelengths selected by SPA, GA, iPLSR and siPLSR all had good prediction performance, among which GA and siPLSR had better prediction performance. 3) The spectral range of 600-750 nm, 1020-1120 nm, 1450-1570 nm had better correlation with TVB-N value, which could be used to establish a multi-spectral system for pork freshness. 4) The performance of the visualization model was inconsistent with that of the spectral model, and the TVB-N content distribution maps generated by the spectral model with similar performance had a huge difference. 5) Visualization could be greatly improved by reducing the number of principal component factors of PLSR and finding a balance between visual evaluation parameters and spectral model performance. This work could lay a theoretical foundation for the establishment of a multi-spectral imaging system suitable for agricultural product detection, and provide a new method for evaluating and optimizing the visualization effect.

References

- Alfaia, C. M., Lopes, P. A., Madeira, M. S., Pestana, J. M., Coelho, D., Toldrá, F., & Prates, J. A. M. (2019). Current feeding strategies to improve pork intramuscular fat content and its nutritional quality. *Advances in Food and Nutrition Research*, 89, 53-94. <http://dx.doi.org/10.1016/bs.afnr.2019.03.006>. PMID:31351530.
- Antequera, T., Caballero, D., Grassi, S., Uttaro, B., & Perez-Palacios, T. (2021). Evaluation of fresh meat quality by hyperspectral imaging (HSI), nuclear magnetic resonance (NMR) and magnetic resonance

- imaging (MRI): a review. *Meat Science*, 172, 108340. <http://dx.doi.org/10.1016/j.meatsci.2020.108340>. PMID:33129061.
- Baek, I., Lee, H., Cho, B. K., Mo, C., Chan, D. E., & Kim, M. S. (2021). Shortwave infrared hyperspectral imaging system coupled with multivariable method for TVB-N measurement in pork. *Food Control*, 124, 107854. <http://dx.doi.org/10.1016/j.foodcont.2020.107854>.
- Chen, Y., Huang, T. Z., & Zhao, X. L. (2018). Destriping of multispectral remote sensing image using low-rank tensor decomposition. *IEEE Journal of Selected Topics in Applied Earth Observations and Remote Sensing*, 11(12), 4950-4967. <http://dx.doi.org/10.1109/JSTARS.2018.2877722>.
- Cui, H., Dong, Y., Lu, T., Zou, X., Wang, M., Yang, X., & Zhou, H. (2021). Effect of ethanolic extract from *Morus alba* L. leaves on the quality and sensory aspects of chilled pork under retail conditions. *Meat Science*, 172, 108368. <http://dx.doi.org/10.1016/j.meatsci.2020.108368>. PMID:33229104.
- Cui, H., Karim, N., Jiang, F., Hu, H., & Chen, W. (2022). Assessment of quality deviation of pork and salmon due to temperature fluctuations during superchilling. *Journal of Zhejiang University. Science. B.*, 23(7), 578-586. <http://dx.doi.org/10.1631/jzus.B2200030>. PMID:35794687.
- Duffy, S. K., Kelly, A. K., Rajauria, G., Jakobsen, J., Clarke, L. C., Monahan, F. J., Dowling, K. G., Hull, G., Galvin, K., Cashman, K. D., Hayes, A., & O'Doherty, J. V. (2018). The use of synthetic and natural vitamin D sources in pig diets to improve meat quality and vitamin D content. *Meat Science*, 143, 60-68. <http://dx.doi.org/10.1016/j.meatsci.2018.04.014>. PMID:29715661.
- Duong, C., Sung, B., Lee, S., & Easton, J. (2022). Assessing Australian consumer preferences for fresh pork meat attributes: a best-worst approach on 46 attributes. *Meat Science*, 193, 108954. <http://dx.doi.org/10.1016/j.meatsci.2022.108954>. PMID:36041289.
- Frank, D., Zhang, Y., Li, Y., Luo, X., Chen, X., Kaur, M., Mellor, G., Stark, J. & Hughes, J. (2019). Shelf life extension of vacuum packaged chilled beef in the Chinese supply chain. A feasibility study. *Meat Science*, 153, 135-143.
- Ghasemi-Varnamkhashi, M., Apetrei, C., Lozano, J., & Anyogu, A. (2018). Potential use of electronic noses, electronic tongues and biosensors as multisensor systems for spoilage examination in foods. *Trends in Food Science & Technology*, 80, 71-92. <http://dx.doi.org/10.1016/j.tifs.2018.07.018>.
- Huang, Y., Lu, R., & Chen, K. (2018). Assessment of tomato soluble solids content and pH by spatially-resolved and conventional Vis/NIR spectroscopy. *Journal of Food Engineering*, 236, 19-28. <http://dx.doi.org/10.1016/j.jfoodeng.2018.05.008>.
- Jiang, H., Yuan, W., Ru, Y., Chen, Q., Wang, J., & Zhou, H. (2022). Feasibility of identifying the authenticity of fresh and cooked mutton kebabs using visible and near-infrared hyperspectral imaging. *Spectrochimica Acta. Part A: Molecular and Biomolecular Spectroscopy*, 282, 121689. <http://dx.doi.org/10.1016/j.saa.2022.121689>. PMID:35914356.
- Kademi, H. I., Ulusoy, B. H., & Hecer, C. (2019). Applications of miniaturized and portable near infrared spectroscopy (NIRS) for inspection and control of meat and meat products. *Food Reviews International*, 35(3), 201-220. <http://dx.doi.org/10.1080/87559129.2018.1514624>.
- Kiala, Z., Odindi, J., & Mutanga, O. (2017). Potential of interval partial least square regression in estimating leaf area index. *South African Journal of Science*, 113(9-10), 1-9. <http://dx.doi.org/10.17159/sajs.2017/20160277>.
- Kucha, C. T., Liu, L., Ngadi, M., & Gariépy, C. (2021). Anisotropic effect on the predictability of intramuscular fat content in pork by hyperspectral imaging and chemometrics. *Meat Science*, 176, 108458. <http://dx.doi.org/10.1016/j.meatsci.2021.108458>. PMID:33647629.
- Leng, Y., Sun, Y., Wang, X., Hou, J., Zhao, X., & Zhang, Y. (2020). Electrical impedance estimation for pork tissues during chilled storage. *Meat Science*, 161, 108014. <http://dx.doi.org/10.1016/j.meatsci.2019.108014>. PMID:31765929.
- Liu, C. X., Xiao, Y. P., Hu, D. W., Liu, J. X., Chen, W., & Ren, D. X. (2019). The safety evaluation of chilled pork from online platform in China. *Food Control*, 96, 244-250. <http://dx.doi.org/10.1016/j.foodcont.2018.09.025>.
- Pereira, P. F., de Sousa Picciani, P. H., Calado, V., & Tonon, R. V. (2021). Electrical gas sensors for meat freshness assessment and quality monitoring: a review. *Trends in Food Science & Technology*, 118, 36-44. <http://dx.doi.org/10.1016/j.tifs.2021.08.036>.
- Ribeiro, J. S., Santos, M. J. M. C., Silva, L. K. R., Pereira, L. C. L., Santos, I. A., da Silva Lannes, S. C., & da Silva, M. V. (2019). Natural antioxidants used in meat products: A brief review. *Meat Science*, 148, 181-188. <http://dx.doi.org/10.1016/j.meatsci.2018.10.016>. PMID:30389412.
- Shen, L., Wang, H., Liu, Y., Liu, Y., Zhang, X., & Fei, Y. (2020). Prediction of soluble solids content in green plum by using a sparse autoencoder. *Applied Sciences (Basel, Switzerland)*, 10(11), 3769. <http://dx.doi.org/10.3390/app10113769>.
- Tan, W. K., Husin, Z., Yasruddin, M. L., & Ismail, M. A. H. (2022). Recent technology for food and beverage quality assessment: a review. *Journal of Food Science and Technology*, 1-14. <http://dx.doi.org/10.1007/s13197-022-05439-8>. PMID:35463865.
- Tang, Y., Wang, X., Xing, X., Li, Z., & Zhao, M. (2021). Prediction and evaluation method of TVB-N values distribution in pork by hyperspectral imaging. *International Journal of Agricultural and Biological Engineering*, 14(4), 270-276. <http://dx.doi.org/10.25165/ij.ijabe.20211404.6278>.
- Torres, I., & Amigo, J. M. (2020). An overview of regression methods in hyperspectral and multispectral imaging. In J. M. Amigo (Ed.), *Hyperspectral imaging (Data Handling in Science and Technology, Chap. 2.8, Vol., 32, pp. 205-230)*. USA: Elsevier. <http://dx.doi.org/10.1016/B978-0-444-63977-6.00010-9>.
- Wang, X., Zhao, M., Ju, R., Song, Q., Hua, D., Wang, C., & Chen, T. (2013). Visualizing quantitatively the freshness of intact fresh pork using acousto-optical tunable filter-based visible/near-infrared spectral imagery. *Computers and Electronics in Agriculture*, 99, 41-53. <http://dx.doi.org/10.1016/j.compag.2013.08.025>.
- Wei, W., Li, H., Haruna, S. A., Wu, J., & Chen, Q. (2022). Monitoring the freshness of pork during storage via near-infrared spectroscopy based on colorimetric sensor array coupled with efficient multivariable calibration. *Journal of Food Composition and Analysis*, 113, 104726. <http://dx.doi.org/10.1016/j.jfca.2022.104726>.
- Xu, Y., Chen, Q., Liu, Y., Sun, X., Huang, Q., Ouyang, Q., & Zhao, J. (2018). A novel hyperspectral microscopic imaging system for evaluating fresh degree of pork. *Korean Journal for Food Science of Animal Resources*, 38(2), 362-375. <http://dx.doi.org/10.5851/kosfa.2018.38.2.362>. PMID:29805285.
- Yang, R., & Kan, J. (2020). Classification of tree species at the leaf level based on hyperspectral imaging technology. *Journal of Applied Spectroscopy*, 87(1), 184-193. <http://dx.doi.org/10.1007/s10812-020-00981-9>.
- Zhang, J., Zou, X., Zhai, X., Huang, X., Jiang, C., & Holmes, M. (2019). Preparation of an intelligent pH film based on biodegradable polymers and roselle anthocyanins for monitoring pork freshness. *Food Chemistry*, 272, 306-312. <http://dx.doi.org/10.1016/j.foodchem.2018.08.041>. PMID:30309548.
- Zhang, X., Jiang, X., Jiang, H., Zhou, H., He, X., Jiang, D., & Zhang, Y. (2022). Design of Portable flour quality safety detector based on diffuse transmission near-infrared spectroscopy. *Guangpuxue Yu Guangpu Fenxi*, 42(4), 1235-1242. [http://dx.doi.org/10.3964/j.issn.1000-0593\(2022\)04-1235-08](http://dx.doi.org/10.3964/j.issn.1000-0593(2022)04-1235-08).

Zhu, Y., Li, C., Cui, H., & Lin, L. (2020). Plasma enhanced-nutmeg essential oil solid liposome treatment on the gelling and storage properties of pork meat batters. *Journal of Food Engineering*, 266, 109696. <http://dx.doi.org/10.1016/j.jfoodeng.2019.109696>.

Zhuang, Q., Peng, Y., Yang, D., Wang, Y., Zhao, R., & Chao, K., & Guo, Q. (2022). Detection of frozen pork freshness by fluorescence hyperspectral image. *Journal of Food Engineering*, 316, 110840. <https://dx.doi.org/10.1016/j.jfoodeng.2021.110840>.